

Manifestation of Majorana modes overlap in the Aharonov-Bohm effect

S V Aksenov

Kirensky Institute of Physics, Federal Research Center KSC SB RAS,
Akademgorodok street 50/38, 660036 Krasnoyarsk, Russia

E-mail: asv86@iph.krasn.ru

Abstract.

One of the key features of the Majorana bound states emerging in topological superconducting (SC) wires is increasing oscillations of their energy under the growth of magnetic field or chemical potential due to concomitant enhancement of hybridization of the Majorana mode wave functions initially localized at the opposite edges of the structure. In this study we found that the other consequence of it is a shift of Aharonov-Bohm (AB) oscillations of linear-response conductance in an interference device where two ends of the SC wire connected with a normal contact via non-SC wires (arms). In addition, it is accompanied by an oscillation period doubling. The numerical calculations for the spinful system are supported by the analytical results for different spinless models allowing to track the conductance evolution as the hybridization of the Majorana modes increases. It is shown that since the coupling between the different arms and normal contact is implemented only via the different-type Majoranas the AB oscillations acquire a fundamental $\pi/2$ shift in comparison with the effect for an analogous system of zero-energy quantum dots.

PACS numbers: 71.10.Pm, 74.45.+c, 74.78.Na

Keywords: Aharonov-Bohm effect, spin-orbit interaction, topological superconductivity, Majorana bound state, Majorana mode, quantum dot, Kitaev chain

1. Introduction

Starting from theoretical works [1, 2] hybrid semiconducting/superconducting (SC) nanowires have become one of the most prospective systems where the Majorana bound states are being sought. It is proposed that in order to achieve an effective p-wave pairing, which is a key factor in the basic spinless model studied by Kitaev [3], one has to combine a spin-orbit interaction, Zeeman splitting and s-type superconductivity [4, 5]. First experiments on the local tunneling spectroscopy of InAs, InSb semiconducting nanowires possessing a large Rashba parameter and g-factor and being in contact with a superconductor revealed a zero-bias peak in conductance if the magnetic field exceeded some critical value [6]. The effect was initially attributed to the emergence of zero-energy Majorana quasiparticle.

The further progress in epitaxial growth of the hybrid nanowires allowed to synthesize the samples with uniform and clean interfaces between an SC shell and semiconducting core. It led to the hard SC gap induced by the proximity effect [7, 8] and allowed to approach the theory predicted $2G_0$ -height ($G_0 = e^2/h$ - the conductance quantum) of the zero-bias peak [9, 10, 11]. In spite of these advantages the nearly quantized peaks measured in the experiments are not sufficiently stable upon the variation of gate voltage and magnetic field [10, 12] and can be related to the presence of trivial Andreev bound states which are rather ubiquitous in the inhomogeneous wires [13, 14]. Moreover, other transport peculiarities related to the Majorana excitation have not been observed in practice yet. For example, the linear-response conductance resonances of two contacts coupled to the opposite ends of the wire have to be correlated provided by the nonlocality of Majorana bound state [11]. The measurement of nonlocal conductance should represent the features of the bulk-gap closing and reopening [15, 16].

If the lengths of Majorana-state localization (inversely proportional to the induced gap) and SC part of the wire are comparable quantities the Zeeman-field dependence of conductance should demonstrate increasing oscillations when the strength of magnetic field grows up. Such a behavior takes place due to the overlap of wave functions of the Majorana modes (hereinafter, it is assumed that the Majorana bound state consists of two Majorana modes) [17, 18]. The experiment [18] revealed that the oscillations decay or

remain pinned at zero energy.

Many mechanisms were suggested to explain this discrepancy between the theory and experiment. The absence of oscillations can be caused by the Coulomb interaction [19] or inverse proximity effect due to drain lead coupled to the SC material [20]. The decaying oscillations, anticrossings or monotonous decay can arise because of magnetic-field orbital effects [21], nonuniform pairing potential [22], nonuniform Rashba field [23] or the combined influence of temperature, multiple subbands and the simultaneous presence of Majorana and Andreev bound states in the SC wire [24].

Different interference setups have been proposed to detect the nontrivial phase in the SC nanowire. If it is embedded in one of the arms of Aharonov-Bohm (AB) ring, then the Majorana excitation permits to transfer individual electrons and holes instead of Cooper pairs resulting in the change of the magnetoconductance oscillation period [25, 26, 27] and generation of the h/e harmonic of flux-independent persistent current [28, 29]. The ways to distinguish between the Majorana and Andreev bound states were analyzed as well [30, 31, 27]. Some studies were focused on the features of nonlocal transport through a quantum dot, where the topological SC wire plays the role of a structure side-attached to the main channel by both ends, i.e. having a Π -shape. [32, 33].

Here we propose the other way to test the overlap of the Majorana wave functions utilizing interference transport scheme. The setup sketched in Fig.1 includes a massive normal contact coupled with a Π -shape semiconducting wire partly covered by an SC material. The magnetic field is applied to this directly-grounded SC area allowing to switch between the trivial and nontrivial phases. Nonlocal transport properties of the similar devices (that implies two normal contacts) have been already investigated [34, 35, 36]. However, the AB effect and its differences for nonoverlapping and overlapping Majorana modes, $b_{1,2}$, (NOMMs and OMMs, respectively) were not considered. This study is devoted to these issues.

The rest of article is organized as follows. In Sec.2.1 we describe a spinful model of the interference device and present a theory of quantum transport based on the nonequilibrium Green's functions (GFs). Sec. 2.2 is devoted to the numerical analysis of transport properties of the spinful model in the linear-response regime. In Sec.3.1 an analytical

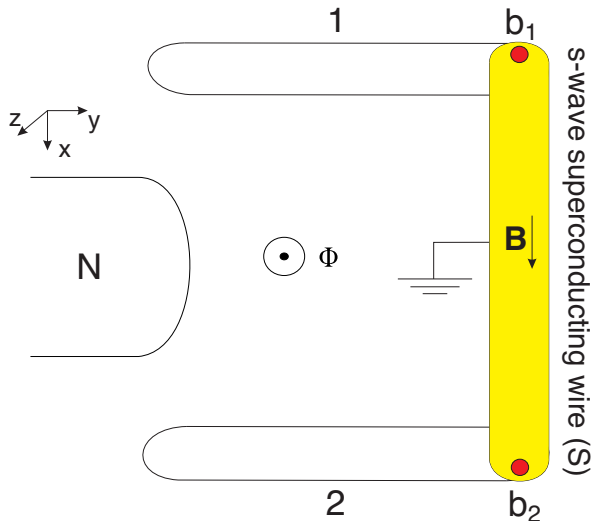


Figure 1. Sketch of an II-shape interference device. It is partly covered by an s-wave superconductor. The sections left uncovered form top (1) and bottom (2) arms which connect the two ends of the directly-grounded superconducting segment (S) with a massive normal contact (N). A magnetic field, \mathbf{B} , is applied locally parallel to the superconducting wire controlling its topological phase. In the nontrivial phase two Majorana modes, b_1 and b_2 , emerge at the opposite edges of the wire as indicated by small red circles. A magnetic flux, Φ , piercing the device plane induces the Aharonov-Bohm oscillations of conductance of the normal contact.

expression of conductance for a spinless model of the interference device is obtained. In Secs.3.2–3.4 we discuss the AB effect differences in the situations of nonoverlapping, weakly hybridizing and overlapping Majorana modes, respectively. We conclude in Sec.4 with a summary. In Appendix A equations of motions (EOMs) and retarded GFs for different low-energy models of the spinless interference device are provided. In Appendix B transport properties of an interferometer containing zero-energy quantum dots (QDs) are numerically studied.

2. Spinful interference system

2.1. Hamiltonian and transport equations

One can treat the system under consideration as the normal (N) and superconducting (S) contacts coupled by the top (1) and bottom (2) arms, which are one-dimensional normal wires, as it is schematically depicted in Fig. 1. The model Hamiltonian has a following general form:

$$\hat{H} = \hat{H}_N + \hat{H}_D + \hat{H}_t. \quad (1)$$

The summand \hat{H}_N characterizes the single-band normal contact,

$$\hat{H}_N = \sum_{k\sigma} \left(\xi_k - \frac{eV}{2} \right) c_{k\sigma}^+ c_{k\sigma}, \quad (2)$$

where $c_{k\sigma}$ - an annihilation operator of the electron with momentum k , spin σ and energy $\xi_k = \varepsilon_k - \mu$ in the contact; μ - a chemical potential of the system; eV - an electric-field energy related to bias voltage. The second term is a tight-binding Hamiltonian which models a device consisting of two normal wires (or top and bottom arms) coupled to the opposite ends of the SC wire, $\hat{H}_D = \hat{H}_1 + \hat{H}_2 + \hat{H}_S + \hat{H}_\tau$,

$$\hat{H}_i = \xi_i \sum_{\sigma; j=1}^{N_i} d_{ij\sigma}^+ d_{ij\sigma} - \quad (3)$$

$$- \sum_{j=1}^{N_i-1} \left(\frac{t_i}{2} d_{ij\sigma}^+ d_{i,j+1,\sigma} + i \frac{\alpha_i^x}{2} d_{ij\sigma}^+ d_{i,j+1,\bar{\sigma}} + H.c. \right),$$

$$\hat{H}_S = \sum_{j=1}^N \left[\xi_S \sum_{\sigma} a_{j\sigma}^+ a_{j\sigma} - h a_{j\uparrow}^+ a_{j\downarrow} + \Delta (a_{j\uparrow} a_{j\downarrow} + H.c.) \right] -$$

$$- \sum_{\sigma; j=1}^{N-1} \left[\frac{t}{2} a_{j\sigma}^+ a_{j+1,\sigma} + \frac{\alpha^y}{2} \sigma a_{j\sigma}^+ a_{j+1,\bar{\sigma}} + H.c. \right], \quad (4)$$

$$\hat{H}_\tau = - \sum_{\sigma} \left(\frac{\tau_1}{2} d_{1,N_1,\sigma}^+ a_{1\sigma} + \frac{\tau_2}{2} d_{21\sigma}^+ a_{N\sigma} + \right. \quad (5)$$

$$\left. + i \frac{\alpha_i^x}{2} d_{1,N_1,\sigma}^+ a_{1\bar{\sigma}} - i \frac{\alpha_i^x}{2} d_{21\sigma}^+ a_{N\bar{\sigma}} + H.c. \right),$$

where $\xi_i = \varepsilon_i - \mu$, t_i , α_i^x - a single-electron energy, hopping parameter and intensity of the Rashba spin-orbit interaction in the i th arm ($i = 1, 2$), respectively; $\xi_S = \varepsilon - \mu$, t , α^y - the analogous quantities in the SC segment of the device; Δ - a strength of SC pairing induced by the proximity effect; τ_i - a parameter of hopping between the i th arm and SC wire; h - the Zeeman splitting energy caused by the longitudinal magnetic field, \mathbf{B} (see Fig. 1). Note that to realize the topologically nontrivial phase and the Majorana modes, b_1 and b_2 , the magnetic field has to be oriented perpendicular to the vector of effective Rashba field in the SC segment [1, 2]. The SC wire and i th arm contains N and N_i sites, respectively.

The last term in (1) takes into account tunneling processes between the normal contact and structure,

$$\hat{H}_t = \sum_{k\sigma} c_{k\sigma}^+ \left(t_1 e^{-i\frac{\phi}{2}} d_{11\sigma} + t_2 e^{i\frac{\phi}{2}} d_{2,N_2,\sigma} \right) + H.c., \quad (6)$$

where $t_{1,2}$ - intensities of tunnel couplings; $\phi = 2\pi\Phi/\Phi_0$ - the AB phase induced by a magnetic flux Φ penetrating the device; $\Phi_0 = h/e$ - the flux quantum.

To calculate a stationary charge current in the normal contact, $I = e \frac{\partial}{\partial t} \sum_{k\sigma} \langle c_{k\sigma}^+(t) c_{k\sigma}(t) \rangle$, the Hamiltonian (1) is diagonalized based on the Gorkov-Nambu operators [37, 38], $\hat{f}_l = \left(f_{l\uparrow}, f_{l\downarrow}^+, f_{l\downarrow}, f_{l\uparrow}^+ \right)^T$, where $f_{l\sigma}$ - the second quantization operator of particle in one of the four above-described subsystems, l - an index of site or wave vector. Matrix nonequilibrium GFs [39] for the introduced field operators can be

defined as $\hat{G}_{lm}^{ab}(\tau_a, \tau_b) = -i \langle T_K \hat{f}_l(\tau_a) \hat{f}_m^+(\tau_b) \rangle$, where T_K - an operator of time ordering on the Keldysh contour. The indices $a, b = +, -$ of the GFs indicate that the time argument of the corresponding operator belongs to either lower or upper branch of the Keldysh contour.

Performing a series of transformations, the following expression for the current is obtained [40, 41]:

$$I = \frac{2e}{h} \sum_{i,j=1,2} \int_{-\infty}^{+\infty} d\omega \text{Tr} \left[\hat{\sigma} \text{Re} \left\{ \hat{\Sigma}_{ij}^r(\omega) \hat{G}_{ji}^{+-}(\omega) + \right. \right. \quad (7)$$

$$\left. \left. + \hat{\Sigma}_{ij}^{+-}(\omega) \hat{G}_{ji}^a(\omega) \right\} \right],$$

where $\hat{\sigma} = \text{diag}(1, -1, 1, -1)$. The matrix blocks of the device's advanced GF, \hat{G}_{ji}^a , are determined by the solution of the Dyson equation,

$$\hat{G}^a = \left[(\omega - \hat{h}_D - \hat{\Sigma}^r(\omega))^{-1} \right]^+, \quad (8)$$

where $\hat{\Sigma}^r(\omega)$ - a matrix of the retarded self-energy function reflecting the influence of the contact on the device. Assuming that the normal contact band is wide, one has the following nonzero blocks of $\hat{\Sigma}^r(\omega)$:

$$\hat{\Sigma}_{11(22)}^r = -\frac{i}{2} \hat{\Gamma}_{11(22)}, \quad \hat{\Sigma}_{21(12)}^r = -\frac{i}{2} \hat{\Gamma}_{12} \hat{\Phi}_{\pm}^2, \quad (9)$$

$$\hat{\Phi}_{\pm} = \text{diag} \left(e^{\pm i \frac{\phi}{2}}, e^{\mp i \frac{\phi}{2}}, e^{\pm i \frac{\phi}{2}}, e^{\mp i \frac{\phi}{2}} \right),$$

where $\hat{\Gamma}_{ii} = \Gamma_i \hat{\tau}_0$, $\Gamma_i = 2\pi\rho(t_i/2)^2$ - functions characterizing the broadening of the device levels ($i = 1, 2$); $\hat{\tau}_0$ - an 4×4 identity matrix; ρ - the contact density of states; $\Gamma_{12} = \sqrt{\Gamma_1 \Gamma_2}$. The matrix lesser GF, \hat{G}_{ij}^{+-} , in (7) is found from the solution of the Keldysh equation, $\hat{G}^{+-} = \hat{G}^r \hat{\Sigma}^{+-} \hat{G}^a$. Its nonzero blocks are

$$\hat{\Sigma}_{ij}^{+-} = -2\hat{\Sigma}_{ij}^r \cdot \text{diag}(n_h, n_e, n_h, n_e), \quad i, j = 1, 2, \quad (10)$$

where $n_{e(h)} \equiv n(\omega \mp eV/2)$ - the Fermi-Dirac distribution functions.

2.2. Results of numerical calculation

For simplicity, in the following numerical analysis we will assume that $\xi_1 = \xi_2$, $t_1 = t_2 = t$, $N_1 = N_2$. At the same time, to study the influence of spin-orbit coupling in the arms on the AB effect in more details the cases of identical and different normal wires will be analyzed separately, namely: 1) $\alpha_1^x = -\alpha_2^x = \alpha^x$; 2) $\alpha_1^x = -2\alpha_2^x = \alpha^x$. In order to model real InAs, InSb semiconducting wires of μm length the lattice constant is chosen as $a = 50$ nm. Then, using the effective mass value found experimentally, $m = 0.015m_0$, the hopping parameter is $t = \hbar^2/ma^2 \approx 2$ meV [6]. Throughout all the numerical calculations the other energy parameters are measured in the units of t . Namely, $\varepsilon_{1,2} = 0$, $\varepsilon = 1$,

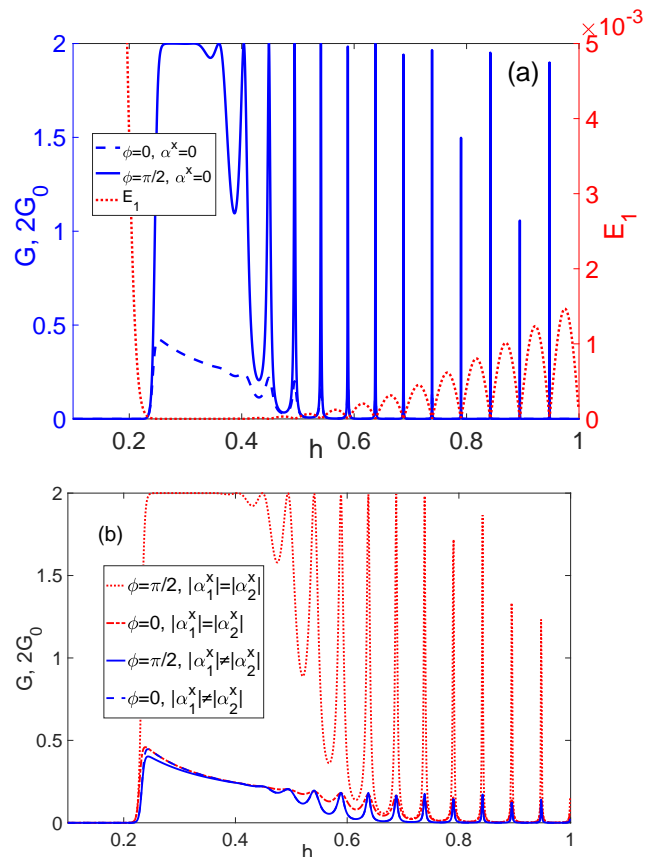


Figure 2. Zeeman-field dependence of conductance for the zero (dashed curves) and nonzero (solid curves) Aharonov-Bohm phase if (a) $\alpha^x = 0$ or (b) $\alpha^x \neq 0$. The lowest excitation energy of the device as a function of the Zeeman energy is plotted in Fig. (a) by dotted curve (see right y axis).

$\mu = 0$, $\Delta = 0.2$, $\alpha^x = 0.4$, $\alpha^y = 0.3$, $\Gamma_{1,2} = 0.01$, $\tau_{1,2} = 0.1$, $k_B T \approx 0$, $N_1 = 30$ and $N = 60$.

To extract the effect related to the presence of SC segment in the device on low-energy interference transport we start with the limiting case when $\alpha^x = 0$. The corresponding Zeeman-energy dependence of conductance is shown in Fig. 2a. The behavior of $G(h)$ for the zero (dashed curve) and nonzero (solid curve) magnetic flux is qualitatively similar. At the low fields, $h < \Delta$, the SC wire is in the trivial phase and the energy of the device lowest state, E_1 , is nonzero (see dotted curve) leading to $G = 0$. In opposite, if $h > \Delta$ the phase is nontrivial. At the intermediate magnetic fields, close to the critical one, $E_1 \approx 0$ resulting in the monotonous dependence of $G(h)$. At $\phi = \pi/2$ the conductance reaches $4G_0$ value implying that both Majorana modes are involved in the transport between the normal and superconducting contacts contributing $2G_0$ each,

$$b_1 = \sum_{\sigma; j=1}^{N+2N_1} w_{j\sigma} \gamma_{j\sigma A}, \quad b_2 = \sum_{\sigma; j=1}^{N+2N_1} z_{j\sigma} \gamma_{j\sigma B}, \quad (11)$$

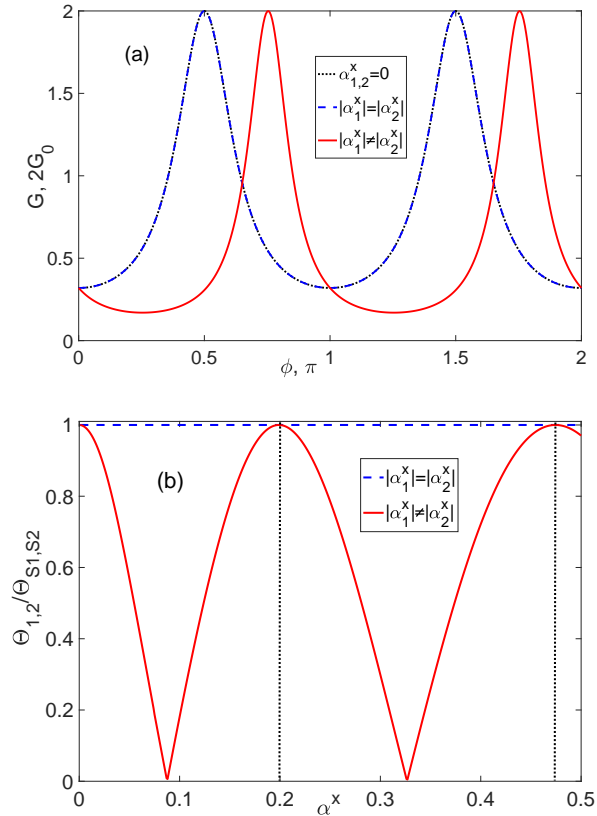


Figure 3. (a) Aharonov-Bohm oscillations of conductance for nonoverlapping Majorana modes. (b) Ratio of angles between the spins at the edges of the device, $\Theta_{1,2}$, and at the opposite ends of the SC wire, $\Theta_{S1,S2}$, for the Majorana bound state. The vertical dotted lines indicate the values of α^x for which the maxima of $G(\phi)$ occur at $\phi = \pi(n + 1/2)$, $n \in \mathbb{Z}$. Parameters: $h = 0.31$.

$$w_{j\sigma} = v_{j\sigma}^* + u_{j\sigma}, \quad z_{j\sigma} = i(v_{j\sigma}^* - u_{j\sigma}), \quad (12)$$

where $u_{j\sigma}$, $v_{j\sigma}$ - the spin-dependent Bogoliubov coefficients of the device lowest excitation; $\gamma_{j\sigma A(B)} = \gamma_{j\sigma A(B)}^+$ - the Majorana operators of type A(B). At the high fields the hybridization of Majorana wave functions becomes nonzero giving rise to the oscillations of $E_1(h)$ and $G(h)$.

At zero AB phase the conductance is significantly suppressed. If the spin-orbit coupling in the arms is taken into account and $|\alpha_1^x| = |\alpha_2^x|$ that there is a slight quantitative difference from the $\alpha^x = 0$ case (e.g., compare the solid curve in Fig. 2a with the dotted curve in Fig. 2b). When $|\alpha_1^x| \neq |\alpha_2^x|$ the divergence can be significant, which is especially prominent at $\phi = \pi/2$ (see solid curve in Fig. 2b).

The AB oscillations of conductance are plotted in Fig. 3a when the device is in the nontrivial phase with the NOMMs. Both at $\alpha^x = 0$ and at $\alpha^x \neq 0$, $|\alpha_1^x| = |\alpha_2^x|$ the peaks appear when $\phi = \pi(n + 1/2)$, $n \in \mathbb{Z}$ (see dotted and dashed curves). In turn, the

different spin-orbit interaction in the arms leads to their shift as shown by solid curve.

In general, spin-orbit coupling in the system results in electron spin precession around the Rashba vector. Then, an additional phase carriers acquire in such media propagating from j th to j' th site [42] can be related to the change of the angle between the spins of the device lowest excitation, ψ_1 , at these sites, $\Theta(\mathbf{S}_1(j), \mathbf{S}_1(j'))$, where

$$\mathbf{S}_1(j) = \psi_1^\dagger(j) \boldsymbol{\sigma} \frac{\tau_0 + \tau^z}{2} \psi_1(j). \quad (13)$$

Here $\boldsymbol{\sigma} = (\sigma^x, \sigma^y, \sigma^z)$, τ^z - the Pauli matrices acting in the spin and particle-hole space, respectively.

In the presence of mirror symmetry ($\alpha^x = 0$ or $\alpha^x \neq 0$, $|\alpha_1^x| = |\alpha_2^x|$) the angles between the spins at the opposite ends of the SC section, $\Theta(\mathbf{S}_1(j = N_1 + 1), \mathbf{S}_1(j = N_1 + N)) \equiv \Theta_{S1,S2}$, and at the edges of the device, $\Theta(\mathbf{S}_1(j = 1), \mathbf{S}_1(j = 2N_1 + N)) \equiv \Theta_{1,2}$, are the same. The latter is clearly seen in Fig. 3b where a ratio $\Theta_{1,2}/\Theta_{S1,S2}$ as a function of α^x is displayed (see dashed line). On the contrary, if $|\alpha_1^x| \neq |\alpha_2^x|$ the angles match only for the certain values of α^x (see vertical dotted lines in Fig. 3b). Outside these points of the parametric space the conductance resonances appear at $\phi \neq \pi(n + 1/2)$ (see solid curve in Fig. 3a).

One of the main results of this study is displayed in Fig. 4a. As the Zeeman energy increases the positions of the maxima in the AB effect change and the oscillation period doubles. This process is accompanied by the increasing overlap of the Majorana wave functions. The corresponding probability densities, $M_1(j) = \sum_\sigma |w_{j\sigma}|^2$ and $M_2(j) = \sum_\sigma |z_{j\sigma}|^2$, are shown in Fig. 4b,c for $|\alpha_1^x| \neq |\alpha_2^x|$ at intermediate and high magnetic fields, respectively. To observe such a hybridization in transport the modes must have nonzero probability density at both ends of the device. In order for the leakage of Majorana modes [43] into the arms to be possible in our system, the normal wires have to be quantum wells, $\varepsilon_{1,2} \leq \varepsilon$. Then, the desired situation of $M_1(N + 2N_1)$, $M_2(1) \neq 0$ realizes at the high magnetic fields as it can be seen from Fig. 4d where the h -dependencies of $M_1(1)$ and $M_1(N + 2N_1)$ are plotted (the b_2 mode behaves identically). In the trivial phase ($h < 0.2$ or $h > 2$) the device lowest-energy excitation is localized in one of the arms since $|\alpha_1^x| \neq |\alpha_2^x|$ leading to either $M_1(1) = 0$ or $M_1(N + 2N_1) = 0$. Immediately before the topological phase transition the $M_1(j)$ is mostly concentrated in the SC section causing its sudden drop at both edges of the device. In the nontrivial phase at the intermediate fields ($0.2 < h \lesssim 0.5$) the $M_1(j)$ is localized predominantly at the boundary of the SC wire and arm 1 (see Fig. 4b). Then, at the high fields, $0.5 \lesssim h < 2$, the process of b_1 delocalization results in $M_1(N + 2N_1) \neq 0$ at the expense of the $M_1(1)$

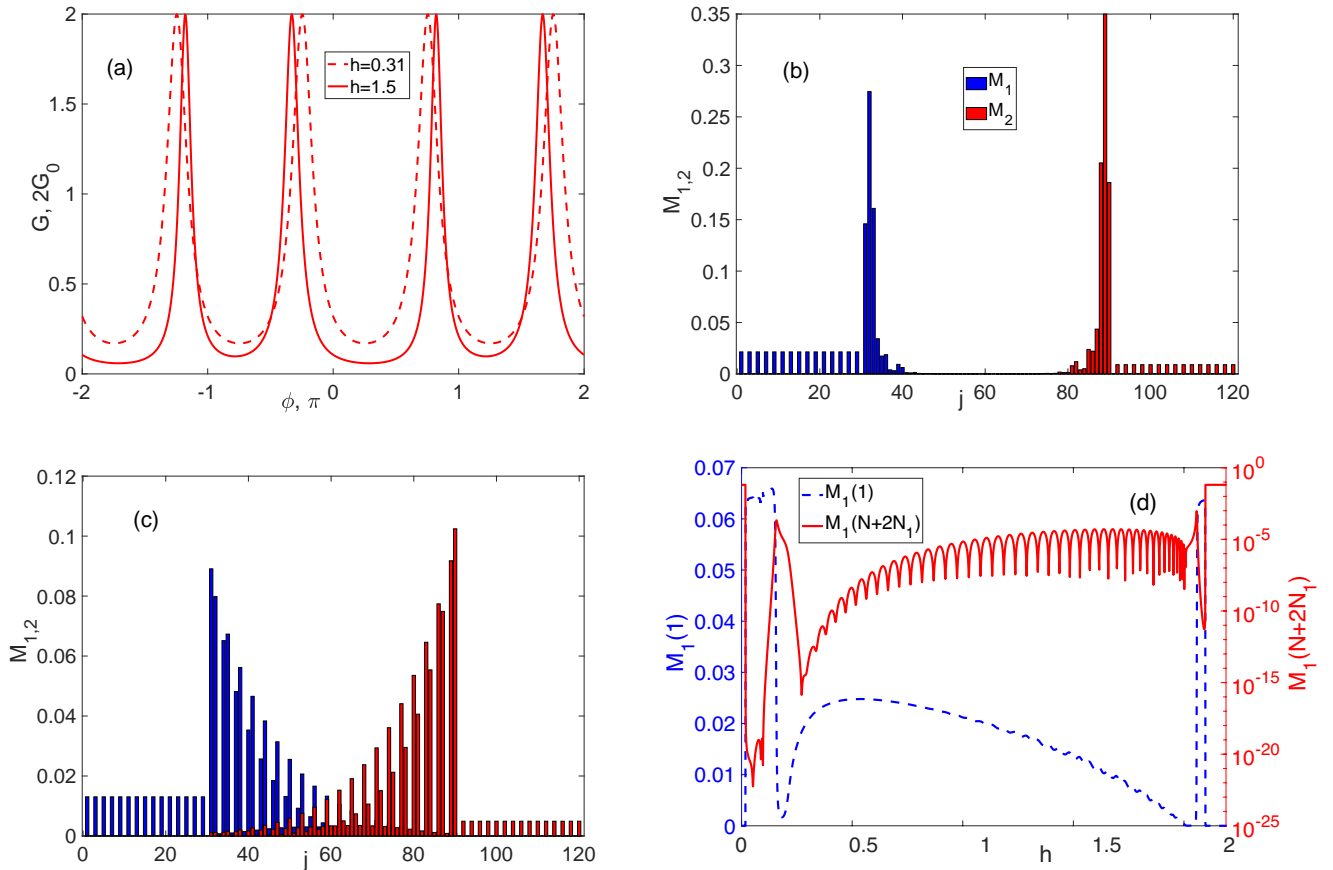


Figure 4. (a) Effect of Majorana modes overlap on the Aharonov-Bohm oscillations of conductance. Spatial distribution of the Majorana modes at the intermediate, $h = 0.31$ (b), and high, $h = 1.5$ (c), magnetic fields. (d) Zeeman-energy dependence of b_1 probability density at the top and bottom edge of the structure. Parameters: $|\alpha_1^+| \neq |\alpha_2^+|$.

reduction albeit $M_1(N + 2N_1) \ll M_1(1)$. In turn, it leads to the narrowing of conductance resonant peaks (e.g. see Figs. 2b and 4a).

When the in-plane magnetic field increases the probability density in the central part of the SC wire becomes nonzero at the expense of decrease of the probability density at its ends and the arms.

Note that the described picture seems feasible in the modern experiments since to reach ballistic transport regime the short wires are used ($\sim 0.1 - 1 \mu\text{m}$). Taking additionally into account the available proximity-induced SC gaps ($\sim 0.1 - 1 \text{ meV}$) one can conclude that the Majorana modes are able to extend over the whole structure [11, 16]. In the next section considering a spinless inference system we will analytically show that the direct interaction of the mode $b_{1(2)}$ with the arm 2(1) induces the AB peaks shift.

The proposed setup can be effective in distinguishing between the nontopological quasi-Majorana state and nonlocal topological Majorana state with spatially separated Majorana modes. The former emerge in the

trivial phase due to the presence of smooth electrostatic and/or SC pairing potentials around the N/S interfaces [22, 44, 45]. Despite the fact that in this case the overlap of the Majorana modes can vary significantly and be even comparable with the one in the nontrivial phase, they are still localized in such an inhomogeneous region. As a result, although the linear-response conductance can reach $4G_0$ for this type of states [45] it is difficult to expect the observation of AB oscillations. On the other hand, the OMMs observed at the high magnetic fields can be treated as an ordinary fermionic subgap state featuring a bulk-like spatial distribution. As it is shown above the corresponding AB effect differs from the one for the nonlocal topological Majorana bound state, i.e. in the case of NOMMs.

3. Analytical results for spinless model

3.1. Formula for conductance mediated by local Andreev reflection

To describe analytically the found features of low-energy interference transport let us proceed to the spinless system where the SC segment is represented by the Kitaev chain [3] and the arms are single-level quantum dots (QDs). The device Hamiltonian is

$$\hat{H}_D = \sum_{i=1,2} \xi_i d_i^\dagger d_i - \sum_{j=1}^{N-1} (t a_j^\dagger a_{j+1} - \Delta a_j^+ a_{j+1}^+ + h.c.) - \mu \sum_{j=1}^N \left(a_j^+ a_j - \frac{1}{2} \right) - (\tau_1 d_1^\dagger a_1 + \tau_2 d_2^\dagger a_N + h.c.) \quad (14)$$

For further derivation of the conductance formula in the spinless case it is useful to separate electron and hole degrees of freedom in the normal-metal reservoir. In particular, the frequency-dependent blocks of the retarded and lesser self-energies in (7) can be represented as

$$\hat{\Sigma}_{ji}^r = -\frac{i}{2} \text{diag}(\Gamma_{eji}, \Gamma_{hji}) \equiv -\frac{i}{2} (\hat{\Gamma}_{eji} + \hat{\Gamma}_{hji}), \quad (15)$$

$$\hat{\Sigma}_{ji}^{+-} = i \cdot \text{diag}(\Gamma_{eji} n_e, \Gamma_{hji} n_h) \equiv i (\hat{\Gamma}_{eji} n_e + \hat{\Gamma}_{hji} n_h),$$

where $\Gamma_{eji} = \Gamma_j$, $\Gamma_{e12} = \Gamma_{12} e^{i\phi}$, $\Gamma_{e21} = \Gamma_{e12}^*$, $\Gamma_{hji} = \Gamma_{eji}^*$. The last relations imply $\hat{\Gamma}_{e,h} = \hat{\Gamma}_{e,h}^+$ that, in turn, results in

$$\text{Tr}[\hat{\sigma} \text{Re}\{\hat{\Sigma}^{+-} \hat{G}^a\}] = -\text{Tr}[\hat{\sigma} \hat{\Sigma}^{+-} \hat{G}^r \hat{\Sigma}^r \hat{G}^a]. \quad (16)$$

Using the Keldysh equation and formula (16) the current can be represented by the Landauer-type formula, $I = 2 \frac{e}{h} \int d\omega T_{LAR}(n_h - n_e)$, where the local Andreev reflection (LAR) probability is written as

$$T_{LAR} = \text{Tr} \left[\text{Re} \left\{ \hat{\Gamma}_e \hat{G}^r \hat{\Gamma}_h \hat{G}^a \right\} \right]. \quad (17)$$

The factor 2 in the expression for current appears since both electron and hole degrees of freedom participate at transport. Next, we appeal for the particular structure of the $\hat{G}^{r,a}$ blocks. After some mathematical calculations the LAR transmission becomes

$$T_{LAR} = | e^{i\phi} \Gamma_1 f_{11} + e^{-i\phi} \Gamma_2 f_{22} + \Gamma_{12} (f_{12} + f_{21}) |^2, \quad (18)$$

where $f_{ji} \equiv \langle\langle d_j^+ | d_i^+ \rangle\rangle$ are the Fourier transforms of anomalous retarded GFs. For the sake of brevity, hereinafter the index 'r' denoting retarded character of the response is omitted. In the following we are concentrated on a study of quantum transport in the linear-response regime at the low-temperature limit. Then, the conductance is

$$G = dI/dV = 2G_0 T_{LAR}. \quad (19)$$

Thus, the analysis of transport features reduces to the finding of f_{ji} . In order to solve this problem the EOM technique is utilized for the three cases [46]. The corresponding details are in Appendix A.

3.2. Nonoverlapping Majorana modes

As a starting point we consider the Kitaev chain at the symmetric point, $t = \Delta$ and $\mu = 0$, with the adjacent QDs (the symmetric Kitaev chain, SKC). In this case there are two NOMMs. The substitution of found GFs (A.5) into (18) gives

$$T_{NOMM} = 4t^4 \omega^2 [\Gamma_1^2 \tau_1^4 D_2^2 + \Gamma_2^2 \tau_2^4 D_1^2 - 2\Gamma_1 \Gamma_2 \tau_1^2 \tau_2^2 D_1 D_2 \cos 2\phi] / |Z|^2, \quad (20)$$

where $D_j = C(\omega^2 - \varepsilon_j^2 - \tau_j^2) - \tau_j^2(\omega^2 - \tau_j^2)$, $C = \omega^2 - 4t^2$, $j = 1, 2$.

It is essential to notice that if $\phi = \pi(n + 1/2)$, $n \in \mathbb{Z}$, the GFs have a first-order pole at $\omega = 0$, i.e. $Z = \omega \tilde{Z}$. Then,

$$\tilde{T}_{NOMM} = 4t^4 [\Gamma_1 \tau_1^2 D_2 + \Gamma_2 \tau_2^2 D_1]^2 / |\tilde{Z}|^2, \quad (21)$$

where

$$\tilde{Z} = \omega \left\{ D_1 D_2 - \frac{C}{4} (\Gamma_1^2 D_2 + \Gamma_2^2 D_1 + 2\Gamma_1 \Gamma_2 D_3) \right\} + i \left\{ 2t^2 (\Gamma_1 \tau_1^2 D_2 + \Gamma_2 \tau_2^2 D_1) + \omega^2 [\Gamma_1 (C - \tau_1^2) D_2 + \Gamma_2 (C - \tau_2^2) D_1] \right\}, \quad (22)$$

where $D_3 = C(\omega^2 - \varepsilon_1 \varepsilon_2 - \tau_1^2 - \tau_2^2) + \tau_1^2 \tau_2^2 - 2t^2(\tau_1^2 + \tau_2^2)$. In other words, $\omega = 0$ is an energy of the bound state in continuum. Taking into account the results (20) and (21) the conductance in the NOMM case is

$$G_{NOMM} = \begin{cases} 2G_0, & \phi = \pi(n + 1/2); \\ 0, & \phi \neq \pi(n + 1/2). \end{cases} \quad (23)$$

The revealed behavior is universal as it is independent on the ratio between ε_j , t_j , τ_j ($j = 1, 2$). The obtained results are confirmed by numerics. In Fig. 5a the AB oscillations for the SKC case are displayed by the solid curve.

The found features of conductance coincide with the ones for the situation when there is no QDs between the normal contact and Kitaev chain. The corresponding anomalous GF's are provided in Appendix A2. Using them the LAR-mediated transmission can be expressed as

$$T_0 = \frac{t^4 \omega^2 (\omega^2 - t^2)^2}{4 |Z|^2} [\Delta \Gamma^2 \cos^2 \phi + \Gamma^2 \sin^2 \phi], \quad (24)$$

where $\Delta \Gamma = \Gamma_1 - \Gamma_2$, $\Gamma = \Gamma_1 + \Gamma_2$. Taking into account the phase dependence of the denominator, Z , presented in the formula (A.10) the linear-response conductance is described by the expression (23) and is not affected by the Γ_1/Γ_2 ratio.

It is worth to note that the observed sharp AB oscillations resemble the corresponding conductance behavior of two noninteracting QDs (double quantum

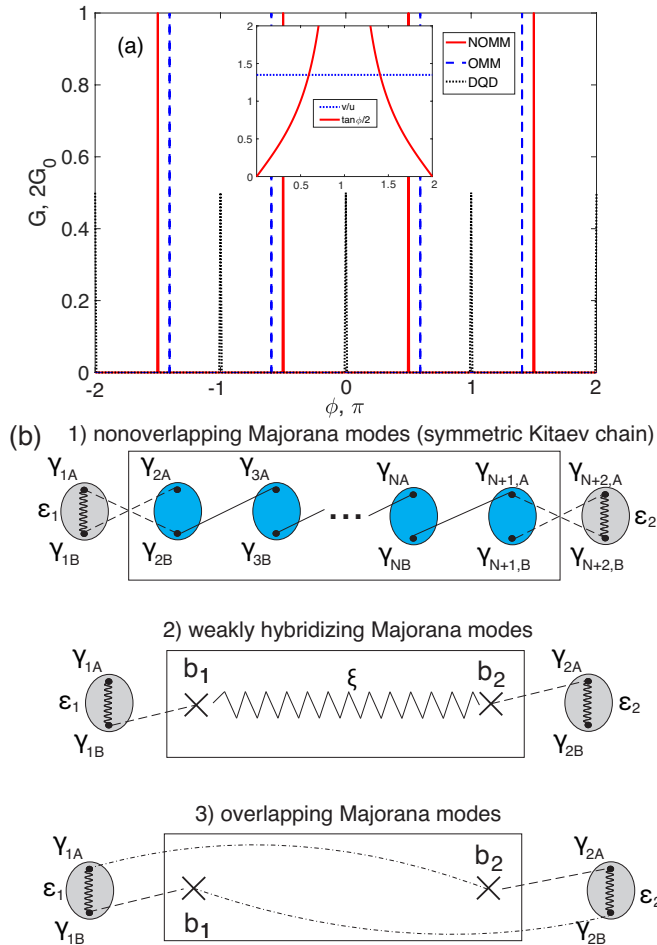


Figure 5. (a) The linear-response conductance of the interference device as a function of the Aharonov-Bohm phase. The maxima emerge at $\phi = \pi(n + 1/2)$ if the Kitaev chain is in the topological phase with the nonoverlapping Majorana modes (see solid curve). The peaks are shifted to the values $\phi = 2 \arctan v/u$ if the Majorana modes overlap (see dashed curve). Inset: the graphic solution of the equation $v/u = \tan \phi/2$. Parameters: $\Gamma_1 = \Gamma_2 = 0.01$, $\tau_1 = \tau_2 = 0.2$, $\varepsilon_1 = \varepsilon_2 = 0$, $\Delta = t = 1$, $\mu = 0$, $N = 20$. To obtain the zero-energy state with the overlapping Majorana modes $\mu \approx 1.97$ and $\Delta = 0.1$ are set. (b) Three types of the device in the Majorana representation.

dot, DQD) between normal contacts in the limiting case $\varepsilon_1 = \varepsilon_2 = 0$ (see black dotted curve in Fig. 5a) [47]. Thus, in the separate SKC (i.e. without the side-attached dots) two decoupled Majorana fermions, γ_{1A} and γ_{NB} , can be treated as such a double-dot structure connected to the electron and hole reservoirs in parallel. However, it is essential that in the case of Majoranas the G maxima are fundamentally shifted by the $\pi/2$ in comparison with the mentioned DQD situation [47] (see blue dashed and black dotted curves in Fig. 5a). This effect is explained by the fact that the same phase carriers acquire tunneling from the contact to the B -type Majorana mode in the bottom arm. Note

that the similar effect was demonstrated in the nonlocal transport through the QD with the side-coupled SKC having the Π -shape [32, 33].

In general, the suggested analogy with two noninteracting QDs is not complete since in our case the other eigenstates having nonzero energies are also able to contribute to the transport. For example, in the simplest situation of SKC directly coupled with the contact two Majorana double-dot molecules (consisting of γ_{1B} , γ_{2A} and $\gamma_{N-1,B}$, γ_{NA} , respectively) also interact with it. Then, both arms of the device include two chains characterized by opposite parity of Majorana-fermion number. Taking it into account in Appendix B we numerically analyzed the transport properties of the analogous AB interferometer containing ordinary zero-energy QDs. It is shown the result (23) can be reproduced for any odd number of QDs in the separate arm (see Appendix B for details).

Hence, it becomes clear why there is no effect of nonzero ε_1 , ε_2 on the conductance features, that can be perceived as another manifestation of the Majorana-mode leakage [43]. The explicit reason of such a behavior is uncovered if the QD-SKC-QD device is considered in the Majorana-operator representation. As it is shown in the top row of Fig. 5b for any $\varepsilon_{1,2}$ there are two uncoupled chains characterized by an odd-parity number of the Majorana fermions connected in series. That, in turn, implies the presence of the two zero-energy eigenstates interacting with the normal contact. Obviously, the oscillations (23) have to keep for the arbitrary number of zero-energy QDs attached to the SKC edges.

3.3. Weakly hybridizing Majorana modes

Now we focus on the SC wire in the nontrivial phase modeled by the effective Hamiltonian $\hat{H}_{eff} = i\xi b_1 b_2/2$, where $\xi \sim e^{-N}$ is a measure of hybridization of the Majorana modes $b_1 = \sum_{j=1}^N w_j \gamma_{jA}$ and $b_2 = \sum_{j=1}^N z_j \gamma_{jB}$ ($b_1 = \gamma_{1A}$, $b_2 = \gamma_{NB}$ if $N \rightarrow \infty$) [3]. As this interaction is supposed to be weak there is no immediate coupling between b_1 (b_2) and the right (left) QD (see the middle row of Fig. 5b). Then, based on the necessary GFs which are brought in Appendix A3, the conductance in the symmetric transport regime (i.e. $\Gamma_1 = \Gamma_2 = \Gamma/2$, $\tau_1 = \tau_2 = \tau$, $\varepsilon_1 = \varepsilon_2 = \varepsilon$) has form

$$G_{eff} = 2G_0 \cdot \Gamma^2 \tau^4 \omega^2 \frac{(\omega^2 - \varepsilon^2 - \tau^2)^2 \sin^2 \phi}{4 |Z|^2}. \quad (25)$$

From expression (A.14) one can easily conclude that for the NOMMs ($\xi = 0$) the conductance at $\omega = 0$ is equal to $2G_0$ if $\phi = \pi(n + 1/2)$, $n \in \mathbb{Z}$. Otherwise, it is zero, that is in complete agreement with the above-obtained result (23). However, the mentioned features

also take place if $\varepsilon = 0$ even though $\xi \neq 0$. The latter can be easily explained if one again refers to the system in the Majorana representation displayed in the middle row of Fig. 5b. Indeed, when on-dot energies $\varepsilon_{1,2}$ are zero two unpaired Majorana fermions, γ_{1A} and γ_{2B} , occur giving rise to one zero-energy state in each arm. In general situation of $\varepsilon, \xi \neq 0$ the linear-response conductance is zero. Mathematically, it means that the first-order pole of the GFs arises at $\omega = 0$ only if $\cos \phi = 2\varepsilon\xi (\pm 2i\varepsilon/\Gamma - 1)/\tau^2$.

3.4. Overlapping Majorana modes

Finally, far from the symmetric point of the Kitaev model, the Majorana zero modes become to hybridize significantly. In particular, it infers that the mode, b_1 or b_2 , initially localized at one of the chain's edges shows the nonzero probability density at the opposite edge. It results in the direct coupling to both QDs with the different amplitudes proportional to $\tau_{1,2}(u \pm v)$ or $\tau_{1,2}(u \mp v)$ (see the dashed and dash-dotted curves in the bottom row of Fig. 5b, respectively) [48, 49]. If $t/\Delta \gg 1$ there are N values of the chemical potential (A.15) at which the zero-energy Bogoliubov excitation with the OMMs emerges. Solving the EOMs (A.20) presented in Appendix A4 one can obtain the following transmission in the symmetric transport regime:

$$T_{OMM} = \frac{4\Gamma^2\tau_e^2\tau_h^2\omega^2(\omega^2 - \varepsilon^2 - 2\tau_p)^2 \sin^2 \phi}{|Z|^2}. \quad (26)$$

Taking into account the ω -dependence of the GFs' denominator (A.21) the linear-response conductance is

$$G_{OMM} = \begin{cases} 2G_0, & \varepsilon = 0 \text{ and } v/u = \tan \phi/2; \\ 0, & \varepsilon \neq 0 \text{ or } v/u \neq \tan \phi/2. \end{cases} \quad (27)$$

The AB oscillations are depicted in Fig. 5a by the dashed curve. According to the expression (27) the maxima appear at the phase values $\phi = 2 \arctan v/u$ (see the graphic solution of the equation $v/u = \tan \phi/2$ in the inset). Note that the positions of conductance peaks tend to $\phi = \pi(n + 1/2)$ if the hybridization of the Majorana modes vanishes meaning the condition $u = v$. Hence, in the OMM situation the AB oscillation period doubles (compare solid and dashed curves in Fig. 5a).

The difference between $\varepsilon \neq 0$ and $\varepsilon = 0$ cases can be readily understood looking at the bottom row of Fig. 5b. If $\varepsilon = 0$ two noninteracting chains emerge each of which is a triple Majorana-dot molecule coupled in parallel with the electron and hole reservoirs. In other words, it again provides the doubly degenerate zero-energy eigenstate of the device. Such a state is absent when $\varepsilon \neq 0$.

4. Summary

In this study we offered a new method to examine the overlap of Majorana modes in the hybrid structure containing the SC segment between the normal wires (arms). In particular, the AB oscillations of linear-response conductance are studied when the normal contact is tunnel coupled with both arms (the Π -shape geometry). As soon as the hybridization of Majorana modes becomes significant the AB resonances shift and the AB oscillation period doubles. The effect emerges since each of the overlapping modes interact with the contact via two arms that is supported by the numerical calculations for the initial spinful model and the analytical analysis for the spinless system including the Kitaev chain and QDs.

Additionally, it is shown that if the factor of spin-orbit interaction in the arms is excluded the conductance peaks related to the perfectly delocalized Majorana bound state occur at $\phi = \pi(n + 1/2)$, $n \in \mathbb{Z}$. It differs from the resonant AB phase $\phi = \pi n$ of the usual interferometer including two uncoupled arms with the odd number of ordinary zero-energy QDs between normal contacts [47]. The reason of this mismatch is that in the former, in fact, the device is coupled to the electron and hole reservoirs by two different-type Majorana operators. By definition, the tunneling phase into them differs by $\pi/2$. In the latter such a feature is absent since the interaction between the contacts and each arm is implemented via the Majorana operators of both types.

Acknowledgments

We acknowledge fruitful discussions with A. D. Fedoseev and M. S. Shustin. The reported study was funded Russian Foundation for Basic Research (project No 20-02-00015), Government of Krasnoyarsk Territory, Krasnoyarsk Regional Fund of Science to the research project "Study of edge states in one- and two-dimensional topological superconductors" (No. 20-42-243005).

Appendix A. The Green's functions of the spinless interference device

In this Appendix the GFs for different SC interference devices coupled to the single normal contact in the spinless regime are brought. To obtain them the EOM technique is applied. A general form of the EOMs for the normal and anomalous retarded frequency-dependent GFs, $\langle\langle d_j | d_i^+ \rangle\rangle \equiv g_{ji}$ and $\langle\langle d_j^+ | d_i^+ \rangle\rangle \equiv f_{ji}$, is

$$(\omega + i\delta) \langle\langle d_j | d_i^+ \rangle\rangle = \langle\{d_j, d_i^+\}\rangle + \langle\langle [d_j, \hat{H}] | d_i^+ \rangle\rangle,$$

$$(\omega + i\delta) \langle\langle d_j^+ | d_i^+ \rangle\rangle = \langle\langle [d_j^+, \hat{H}] | d_i^+ \rangle\rangle. \quad (\text{A.1})$$

The EOM system solution makes it possible to find transmission amplitude associated with LAR processes since

$$t_{LAR} = e^{i\phi} \Gamma_1 f_{11} + e^{-i\phi} \Gamma_2 f_{22} + \Gamma_{12} (f_{12} + f_{21}). \quad (\text{A.2})$$

Thus, the following subsections present the diagonal and off-diagonal anomalous GFs.

1. The symmetric Kitaev chain

In order to treat the transport problem analytically we first address to the Kitaev model at the symmetric point, $t = \Delta$ and $\mu = 0$. Employing the Majorana-operator representation, $a_j = \frac{1}{2}(\gamma_{jA} + i\gamma_{jB})$, where $\gamma_{jA,B} = \gamma_{jA,B}^+$, one can rewrite the device Hamiltonian (14) in the form

$$\begin{aligned} \hat{H}_D = & \sum_{i=1,2} \xi_i d_i^+ d_i + it \sum_{j=1}^{N-1} \gamma_{jB} \gamma_{j+1,A} - \\ & - \frac{\tau_1}{2} [(d_1^+ - d_1) \gamma_{1A} + i(d_1^+ + d_1) \gamma_{1B}] - \\ & - \frac{\tau_2}{2} [(d_2^+ - d_2) \gamma_{2A} + i(d_2^+ + d_2) \gamma_{2B}]. \end{aligned} \quad (\text{A.3})$$

As a result, the EOM system (A.1) for $i = 1$ is $\hat{A}_1 \hat{x}_1 = \hat{B}_1$, where $\hat{x}_1 = (g_{11}, g_{21}, f_{11}, f_{21})^T$. The coefficient matrix and column vector are

$$\begin{aligned} \hat{A}_1 = & \begin{pmatrix} z_{1e} & z_{12} & 2t^2 \tau_1^2 & 0 \\ -z_{12}^* & z_{2e} & 0 & -2t^2 \tau_2^2 \\ 2t^2 \tau_1^2 & 0 & z_{1h} & -z_{12}^* \\ 0 & -2t^2 \tau_2^2 & z_{12} & z_{2h} \end{pmatrix}, \\ \hat{B}_1 = & (\omega C, 0, 0, 0)^T, \end{aligned} \quad (\text{A.4})$$

where $z_{je(h)} = C(\omega C_{je(h)} - \tau_j^2) - 2t^2 \tau_j^2$, $z_{12} = i\omega C \Gamma_{12} e^{i\phi}/2$, $C = \omega^2 - 4t^2$, $C_{je(h)} = \omega \mp \varepsilon_j + i\Gamma_j/2$.

The EOM system for $i = 2$ can be written in a similar manner. Their solution gives the sought anomalous GFs,

$$\begin{aligned} f_{11} = & -\frac{t^2}{2} \cdot \frac{\omega C \tau_2^2 \Gamma_{12}^2 e^{-2i\phi} + 4\tau_1^2 Z_2}{Z}, \\ f_{22} = & \frac{t^2}{2} \cdot \frac{\omega C \tau_1^2 \Gamma_{12}^2 e^{2i\phi} + 4\tau_2^2 Z_1}{Z}, \\ f_{21} = & i\Gamma_{12} t^2 \cdot \frac{\tau_1^2 z_{2e} e^{i\phi} - \tau_2^2 z_{1h} e^{-i\phi}}{Z}, \\ f_{12} = & i\Gamma_{12} t^2 \cdot \frac{\tau_1^2 z_{2h} e^{i\phi} - \tau_2^2 z_{1e} e^{-i\phi}}{Z}, \end{aligned} \quad (\text{A.5})$$

where

$$\begin{aligned} Z_j = & \omega (C C_{je} C_{jh} + \tau_j^4) - \tau_j^2 (C + 2t^2) (C_{je} + C_{jh}), \\ Z = & Z_1 Z_2 + \frac{\Gamma_{12}^2}{4} (z_{1e} z_{2e} + z_{1h} z_{2h} + \omega^2 C^2 \frac{\Gamma_{12}^2}{4} - \\ & - 8t^4 \tau_1^2 \tau_2^2 \cos 2\phi). \end{aligned} \quad (\text{A.6})$$

2. The symmetric Kitaev chain directly coupled to the normal contact

If there are no dots between the contact and Kitaev chain, then in the symmetric point one can easily write the following coefficient matrix and column vector writing the EOMs for the Majorana GFs, $\hat{A}_{1A} \hat{x}_{1A} = \hat{B}_{1A}$, where $\hat{x}_{1A} = (m_{1A,1A}, m_{1B,1A}, m_{NA,1A}, m_{NB,1A})^T$ and $m_{iA,jB} = \langle\langle \gamma_{iA} | \gamma_{jB} \rangle\rangle$:

$$\begin{aligned} \hat{A}_{1A} = & \begin{pmatrix} \hat{D}_1 & \hat{T}_{12} \\ \hat{T}_{12}^T & \hat{D}_2 \end{pmatrix}, \hat{T}_{12} = 2i\Gamma_{12}\omega \begin{pmatrix} \cos \phi & -\sin \phi \\ \sin \phi & \cos \phi \end{pmatrix}, \\ \hat{D}_1 = & \text{diag}(\Omega_1, \omega_1), \hat{D}_2 = \text{diag}(\omega_2, \Omega_2), \\ \hat{B}_{1A} = & (2\omega, 0, 0, 0)^T, \end{aligned} \quad (\text{A.7})$$

where $\Omega_j = \omega \omega_j - t^2$, $\omega_j = \omega + 2i\Gamma_j$. Note that the factor 2 in \hat{B}_{1A} is caused by the nonfermionic anticommutation relations, i.e. $\{\gamma_{iA(B)}, \gamma_{jA(B)}\} = 2\delta_{ij}$. The three systems for the rest of Majorana GFs, i.e. $m_{jA(B),1B}$, $m_{jA(B),2A}$ and $m_{jA(B),2B}$, have similar form. Finally, taking into account the relation between the Majorana and fermionic GF's,

$$f_{ij} = \frac{1}{4} [m_{iA,jA} - m_{iB,jB} - i(m_{iA,jB} + m_{iB,jA})], \quad (\text{A.8})$$

the required anomalous GFs are

$$\begin{aligned} f_{11} = & -\frac{t^2}{2} \cdot \frac{\Omega_2 (\omega + 2i\Gamma_2) + 4\Gamma_{12}^2 \omega e^{2i\phi}}{Z}, \\ f_{22} = & \frac{t^2}{2} \cdot \frac{\Omega_1 (\omega + 2i\Gamma_1) + 4\Gamma_{12}^2 \omega e^{-2i\phi}}{Z}, \\ f_{12} = & f_{21} = \Gamma_{12} t^2 \cdot \frac{2\Delta \Gamma \omega \cos \phi + [\omega (\omega_1 + \omega_2) - t^2] \sin \phi}{Z}, \\ Z = & \omega \Omega [\omega \Omega - 2i\Gamma t^2] - 4\Gamma_{12}^2 t^4 \cos^2 \phi, \end{aligned} \quad (\text{A.9})$$

where $\Gamma = \Gamma_1 + \Gamma_2$, $\Delta \Gamma = \Gamma_1 - \Gamma_2$, $\Omega = \omega^2 + 2i\Gamma\omega - t^2$.

3. The effective model of the Kitaev chain

Let us turn to the effective model of the Kitaev chain in the nontrivial phase which describes two Majorana modes localized at the opposite ends on the chain and weakly interacting with each other [3]. In this case the device Hamiltonian can be written as

$$\begin{aligned} \hat{H}_D = & \sum_{i=1,2} \xi_i d_i^+ d_i + i \frac{\xi}{2} b_1 b_2 - \\ & - \frac{\tau_1}{2} (d_1^+ - d_1) b_1 - i \frac{\tau_2}{2} (d_2^+ + d_2) b_2, \end{aligned} \quad (\text{A.11})$$

where ξ - a hybridization parameter. Hence, the EOM technique leads to

$$\begin{aligned} \hat{A}_1 = & \begin{pmatrix} z_{1e} & Z_{12} & T_1 & T_{12} \\ -Z_{12}^* & z_{2e} & -T_{12} & T_2 \\ T_1 & -T_{12} & z_{1h} & -Z_{12}^* - 2T_{12} \\ T_{12} & T_2 & Z_{12} - 2T_{12} & z_{2h} \end{pmatrix} \\ \hat{B}_1 = & (\omega^2 - \xi^2, 0, 0, 0)^T, \end{aligned} \quad (\text{A.12})$$

where $z_{1e(h)} = (\omega^2 - \xi^2) C_{1e(h)} - T_1$, $z_{2e(h)} = (\omega^2 - \xi^2) C_{2e(h)} - T_2$, $T_{12} = -\xi \tau_1 \tau_2 / 2$, $T_j = \omega \tau_j^2 / 2$, $Z_{12} = i(\omega^2 - \xi^2) \Gamma_{12} e^{i\phi} / 2 + T_{12}$.

Since in the general case \hat{A}_1 has no zero elements the solution of EOM system $\hat{A}_1 \hat{x}_1 = \hat{B}_1$ is more cumbersome. We adduce it for the symmetric transport configuration when $\Gamma_1 = \Gamma_2 = \Gamma/2$, $\tau_1 = \tau_2 = \tau$, $\varepsilon_1 = \varepsilon_2 = \varepsilon$,

$$f_{11(22)} = \pm \frac{\tau^2}{4Z} \left[4\omega (\omega^2 - \tau^2 - \varepsilon^2) + i\Gamma \left(2\omega^2 - \tau^2 - 2\varepsilon\xi e^{\mp i\phi} \mp \frac{\Gamma}{2} \omega e^{\mp i\phi} \sin \phi \right) \right], \quad (\text{A.13})$$

$$f_{21(12)} = \mp \frac{\tau^2}{4Z} \left[4\xi (\omega^2 - \varepsilon^2 + i\Gamma\omega) - 2i\Gamma\varepsilon\omega \cos \phi \mp \Gamma \left(\omega \left(2\omega + i\frac{\Gamma}{2} \right) - \tau^2 \right) \sin \phi \right],$$

where

$$Z = \frac{\Gamma^2}{8} \tau^4 \cos^2 \phi - \tau^4 \omega (2\omega + i\Gamma) - 2(\omega^2 - \xi^2)(\omega^2 - \varepsilon^2) \left[\left(\omega + i\frac{\Gamma}{2} \right)^2 - \varepsilon^2 \right] + \tau^2 (4\omega + i\Gamma) \left[\omega \left(\omega^2 + i\frac{\Gamma}{2} \omega - \varepsilon^2 \right) - i\frac{\Gamma}{2} \varepsilon \xi \cos \phi \right]. \quad (\text{A.14})$$

4. Overlapping Majorana modes

Next, we analyze transport in the device where two QDs coupled in parallel with the single zero-energy Bogoliubov excitation characterized by the significant overlap of the Majorana wave functions. It is well known that the Kitaev chain with N sites has the same number of lines in the parametric space where the lowest excitation energy becomes zero [50], which are defined by the following equations:

$$\mu = 2\sqrt{t^2 - \Delta^2} \cos \frac{\pi m}{N+1}, \quad m = 1, \dots, N. \quad (\text{A.15})$$

The Bogoliubov operators of these zero-energy states, α_m , have form [51]

$$\alpha_m = \frac{1}{S_m} \sum_{j=1}^N r^{j-1} \sin \frac{\pi m j}{N+1} \cdot \left(a_j + a_j^+ + a_{N+1-j} - a_{N+1-j}^+ \right), \quad (\text{A.16})$$

where S_m - a normalization factor; $r = \sqrt{\frac{t-\Delta}{t+\Delta}}$. For concreteness, we consider one of such states, $\alpha_{m=1} \equiv \alpha$. As a result, the u_j and v_j ($j = 1, \dots, N/2$) coefficients are

$$u_j = u_{N+1-j} = \frac{1}{S} r^{j-1} (1 + r^{N-j}) \sin \frac{\pi j}{N+1}, \quad (\text{A.17})$$

$$v_j = -v_{N+1-j} = \frac{1}{S} r^{j-1} (1 - r^{N-j}) \sin \frac{\pi j}{N+1}.$$

Note if $\mu = 0$, then the equations (A.15) and (A.17) obviously lead to the SKC and $u = v$. Consequently, the Majorana-mode operators are $b_1 = \alpha^+ + \alpha = \sum_j w_j \gamma_{jA} = 2u(a_1^+ + a_1)$, $b_2 = i(\alpha^+ - \alpha) = \sum_j z_j \gamma_{jB} = 2iu(a_N^+ - a_N)$. In opposite, if $\mu \neq 0$, then the wave functions related to b_1 and b_2 overlap. The hybridization is stronger if $t/\Delta \gg 1$ resulting in the zero-energy excitation with the bulk spatial distribution.

The inverse Bogoliubov transform gives [30]

$$a_1 \approx u\alpha + v\alpha^+, \quad a_N \approx u\alpha - v\alpha^+, \quad (\text{A.18})$$

where $u \equiv u_1$, $v \equiv v_1$. Then, the structure Hamiltonian is

$$\hat{H}_D = \sum_{i=1,2} \xi_i d_i^+ d_i - (\tau_{1e} d_1^+ + \tau_{2e} d_2^+) \alpha - (\tau_{1h} d_1^+ - \tau_{2h} d_2^+) \alpha^+ + h.c., \quad (\text{A.19})$$

where $\tau_{je} = \tau_j u$, $\tau_{jh} = \tau_j v$.

The EOM coefficient matrix and column vector can be written as

$$\hat{A}_1 = \begin{pmatrix} z_{1e} & Z_{12} & 2T_1 & T_{eh} \\ -Z_{12}^* - 2T_{12} & z_{2e} & T_{eh} & -2T_2 \\ 2T_1 & T_{eh} & z_{1h} & -Z_{12}^* - 2T_{12} \\ T_{eh} & -2T_2 & Z_{12} & z_{2h} \end{pmatrix}, \quad (\text{A.20})$$

$$\hat{B}_1 = (\omega, 0, 0, 0)^T,$$

where $z_{je(h)} = \omega C_{je(h)} - \tau_{je}^2 - \tau_{jh}^2$, $T_j = \tau_{je} \tau_{jh}$, $T_{eh} = \tau_{1h} \tau_{2e} - \tau_{1e} \tau_{2h}$, $T_{12} = \tau_{1e} \tau_{2e} - \tau_{1h} \tau_{2h}$, $Z_{12} = i\Gamma_{12} e^{i\phi}/2 - T_{12}$. The EOM system solution in the symmetric transport regime yields

$$f_{11(22)} = \mp \frac{2\tau_e \tau_h}{Z} \left[i\Gamma e^{-i\phi} \left(2\tau_m \mp \frac{\Gamma}{2} \omega \sin \phi \right) + 2\omega (\omega C - \varepsilon^2) - 2\tau_p (\omega + C) \right],$$

$$f_{21(12)} = \frac{2\tau_e \tau_h}{Z} \left[\Gamma \left(\left(\tau_p - \frac{\omega}{2} (\omega + C) \right) \sin \phi - i\varepsilon \omega \cos \phi \right) \pm 4\tau_m \varepsilon \right],$$

where $C = \omega + i\Gamma/2$, $\tau_{p(m)} = \tau_e^2 \pm \tau_h^2$. The GFs' denominator is

$$Z = \omega^2 (\omega^2 - \varepsilon^2) (C^2 - \varepsilon^2) + 2\omega \left[i\frac{\Gamma}{2} \tau_m (\omega C + \varepsilon^2) \cos \phi - \tau_p (\omega + C) (\omega C - \varepsilon^2) \right] + \left[\tau_p (\omega + C) \cos \phi - i\frac{\Gamma}{2} \tau_m \right]^2 + 4\tau_p^2 \omega C \sin^2 \phi - 4\tau_m^2 \varepsilon^2. \quad (\text{A.21})$$

Appendix B. The Aharonov-Bohm interferometer containing noninteracting arrays of zero-energy quantum dots

In this Appendix let us examine the AB effect in an interference structure of ordinary zero-energy QDs between left and right normal contacts sketched in Fig. B1. The necessity to consider such a system

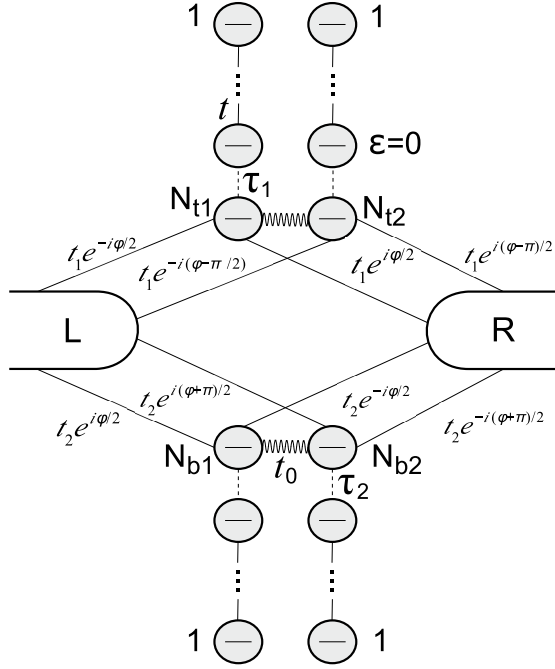


Figure B1. The scheme of the Aharonov-Bohm interferometer including top and bottom noninteracting arrays of zero-energy QDs with $N_{t1} + N_{t2}$ and $N_{b1} + N_{b2}$ elements, respectively.

Table B1. The linear-response conductance of the interferometer sketched in Fig. B1 (in the units of G_0). Parameters: $t, \tau_{1,2}, t_{1,2} \neq 0$.

| | N_{t1} - even, N_{t2} - odd | N_{t1} - odd N_{t2} - even |
|------------------------------------|---|---|
| N_{b1} - even, N_{b2} - odd | 1, $\phi = \pi n$; 0, $\phi \neq \pi n$ | 1, $\phi = \pi(n + 1/2)$; 0, $\phi \neq \pi(n + 1/2)$ |
| N_{b1} - odd, N_{b2} - even | 1, $\phi = \pi(n + 1/2)$; 0, $\phi \neq \pi(n + 1/2)$ | 1, $\phi = \pi n$; 0, $\phi \neq \pi n$ |

is explained by the fact that the interaction between the normal contact and, for example, the SKC implies the coupling with not just the individual Majorana fermions γ_{1A} and γ_{NB} but also with two Majorana molecules including γ_{1B} , γ_{2A} and $\gamma_{N-1,B}$, γ_{NA} , respectively. In the situation of the QD-SKC-QD system the separate sleeve consists of two Majorana-fermion chains with two and three constituents. These chains are coupled when $\varepsilon_j \neq 0$. Thus, if one wants to draw a more explicit analogy between the AB effect in the system of Majorana and fermionic QDs a top (bottom) arm in the latter has to contain two chains with $N_{t1(b1)}$ and $N_{t2(b2)}$ elements of different parity. Additionally, the phase difference of tunneling into these chains is set to $\pi/2$. It allows to show that the behavior (23) takes place if each arm has a single zero-energy eigenstate and the tunneling phase into them differs by $\pi/2$.

To calculate the conductance the expression (17)

can be used where the broadening matrices $\hat{\Gamma}_{e,h}$ have to be replaced by $\hat{\Gamma}_{L,R}$ with the following nonzero blocks:

$$\hat{\Gamma}_{Ljj} = \Gamma_j \hat{\Gamma}_0, \quad \hat{\Gamma}_{L12(21)} = \Gamma_{12} e^{\pm i\phi} \hat{\Gamma}_0, \quad (\text{B.1})$$

$$\hat{\Gamma}_{Rji} = \hat{\Gamma}_{Lji}^*, \quad \hat{\Gamma}_0 = \begin{pmatrix} 1 & i \\ -i & 1 \end{pmatrix}, \quad i, j = 1, 2.$$

The numerical analysis reveals that the result (23) is valid for any random odd (even) $N_{t1,b2}$ and even (odd) $N_{t2,b1}$ (see the colored cells in Table B1). This behavior is not affected by a specific value of t_0 (which is an analogue of $\varepsilon_{1,2}$ and μ in the original spinless device). In other words, the problem is effectively reduced to the model studied in [47] where the real QDs are replaced by two zero-energy eigenstates. For any t_0 there is the only transport path (not two) in each arm involving these states since the corresponding eigenvectors are proportional to $\sin \pi j/2$, where j - a QD number [52]. As a result, if the phase of tunneling into the arms is the same (up to the sign), i.e. the parity of N_{t1} and N_{b1} coincide, the conductance peaks occur at $\phi = \pi n$ [47]. When it differs by $\pi/2$, i.e. N_{t1} and N_{b1} have opposite parity, the corresponding shift appears in the AB effect.

References

- [1] Lutchyn R M, Sau J D and Sarma S D 2010 *Phys. Rev. Lett.* **105** 077001
- [2] Oreg Y, Refael G and von Oppen F 2010 *Phys. Rev. Lett.* **105** 177002
- [3] Kitaev A Y 2001 *Phys. Usp.* **44** 131
- [4] Stanescu T D and Tewari S 2013 *J. Phys.: Condens. Matter* **25** 233201
- [5] Sato M and Ando Y 2017 *Rep. Prog. Phys.* **80** 076501
- [6] Mourik V, Zuo K, Frolov S M, Plissard S R, Bakkers E P A M and Kouwenhoven L P 2012 *Science* **336** 1003
- [7] Chang W, Albrecht S M, Jespersen T S, Kuemmeth F, Krogstrup P, Nygard J and Marcus C M 2015 *Nature Nanotech.* **10** 232
- [8] Pan D, Song H, Zhang S, Liu L, Wen L, Liao D, Zhuo R, Wang Z, Zhang Z, Yang S, Ying J, Miao W, Li Y, Shang R, Zhang H and Zhao J 2020 (*Preprint arXiv:2011.13620*)
- [9] Law K T, Lee P A and Ng T K 2009 *Phys. Rev. Lett.* **103** 237001
- [10] Nichele F, Drachmann A C C, Whitticar A M, O'Farrell E C T, Suominen H J, Fornieri A, Wang T, Gardner G C, Thomas C, Hatke A T, Krogstrup P, Manfra M J, Flensberg K and Marcus C M 2017 *Phys. Rev. Lett.* **119** 136803
- [11] Yu P, Chen J, Gomanko M, Badawy G, Bakkers E P A M, Zuo K, Mourik V and Frolov S M 2021 *Nat. Phys.* **17** 482
- [12] Zhang H, de Moor M W A, Bommer J D S, Xu D, Wang G, van Loo N, Liu C X, Gazibegovic S, Logan J A, Car D, het Veld R L M O, van Veldhoven P J, Koelling S, Verheijen M A, Pendharkar M, Pennachio D J, Shojaei B, Lee J S, Palmstrom C J, Bakkers E P A M, Sarma S D and Kouwenhoven L P 2021 (*Preprint arXiv:2101.11456*)
- [13] Prada E, San-Jose P, de Moor M W A, Geresdi A, Lee E J H, Klinovaja J, Loss D, Nygard J, Aguado R and Kouwenhoven L P 2020 *Nat. Phys. Rev.* **2** 575

- [14] Marra P and Nigro A 2022 *J. Phys.: Condens. Matter* **34** 124001
- [15] Rosdahl T O, Vuik A, Kjaergaard M and Akhmerov A R 2018 *Phys. Rev. B* **97** 045421
- [16] Hess R, Legg H F, Loss D and Klinovaja J 2021 *Phys. Rev. B* **104** 075405
- [17] Sarma S D, Sau J D and Stanescu T D 2012 *Phys. Rev. B* **86** 220506(R)
- [18] Albrecht S M, Higginbotham A, Madsen M, Kuemmeth F, Jespersen T S, Nygard J, Krogstrup P and Marcus C 2016 *Nature* **531** 206
- [19] Dominguez F, Cayao J, San-Jose P, Aguado R, Yeyati A L and Prada E 2017 *npj Quantum Materials* **2** 13
- [20] Danon J, Hansen E B and Flensberg K 2017 *Phys. Rev. B* **96** 125420
- [21] Dmytruk O and Klinovaja J 2018 *Phys. Rev. B* **97** 155409
- [22] Fleckenstein C, Dominguez F, Ziani N T and Trauzettel B 2018 *Phys. Rev. B* **97** 155425
- [23] Cao Z, Zhang H, Lu H F, He W X, Lu H Z and Xie X C 2019 *Phys. Rev. Lett.* **122** 147701
- [24] Chiu C K, Sau J D and Sarma S D 2017 *Phys. Rev. B* **96** 054504
- [25] Benjamin C and Pachos J K 2010 *Phys. Rev. B* **81** 085101
- [26] Akhmerov A R, Dahlhaus J P, Hassler F, Wimmer M and Beenakker C W J 2011 *Phys. Rev. Lett.* **106** 057001
- [27] Whitticar A M, Fornieri A, O'Farrell E C T, Drachmann A C C, Wang T, Thomas C, Gronin S, Kallaher R, Gardner G C, Manfra M J, Marcus C M and Nichele F 2020 *Nat. Com.* **11** 3212
- [28] Buttiker M and Klapwijk T M 1986 *Phys. Rev. B* **33** 5114
- [29] Jacquod P and Buttiker M 2013 *Phys. Rev. B* **88** 241409(R)
- [30] Tripathi K M, Das S and Rao S 2016 *Phys. Rev. Lett.* **116** 166401
- [31] Hell M, Flensberg K and Leijnse M 2018 *Phys. Rev. B* **97** 161401(R)
- [32] Liu D E and Baranger H U 2011 *Phys. Rev. B* **84** 201308(R)
- [33] Ramos-Andrade J P, Orellana P A and Ulloa S E 2018 *J. Phys.: Condens. Matter* **30** 045301
- [34] Shang E M, Pan Y M, Shao L B and Wang B G 2014 *Chin. Phys. B* **23** 057201
- [35] Wang N, Lv S and Li Y 2014 *J. Appl. Phys.* **115** 083706
- [36] Chi F, Wang J, He T Y, Fu Z G, Zhang P, Zhang X W, Wang L and Lu Z 2021 *Front. Phys.* **8** 631031
- [37] Gorkov L P 1958 *Soviet Phys. JETP* **34** 505
- [38] Nambu Y 1960 *Phys. Rev.* **117** 648
- [39] Keldysh L V 1965 *J. Theor. Exp. Phys.* **20** 1018
- [40] Val'kov V V, Kagan M Y and Aksenov S V 2019 *J. Phys.: Condens. Matter* **31** 225301
- [41] Aksenov S V and Kagan M Y 2020 *JETP Lett.* **111** 286
- [42] Bercioux D, Governale M, Cataudella V and Ramaglia V M 2005 *Phys. Rev. B* **72** 075305
- [43] Vernek E, Penteado P H, Seridonio A C and Egues J C 2014 *Phys. Rev. B* **89** 165314
- [44] Penaranda F, Aguado R, San-Jose P and Prada E 2018 *Phys. Rev. B* **98** 235406
- [45] Vuik A, Nijholt B, Akhmerov A R and Wimmer M 2019 *SciPost Phys.* **7** 061
- [46] Zubarev D N 1960 *Sov. Phys. Usp.* **3** 320
- [47] Kubala B and König J 2002 *Phys. Rev. B* **65** 245301
- [48] Prada E, Aguado R and San-Jose P 2017 *Phys. Rev. B* **96** 085418
- [49] Clarke D J 2017 *Phys. Rev. B* **96** 201109(R)
- [50] Hegde S, Shivamoggi V, Vishveshwara S and Sen D 2015 *New J. Phys.* **17** 053036
- [51] Valkov V, Shustin M, Aksenov S, Zlotnikov A, Fedoseev A, Mitskan V and Kagan M 2021 *Phys. Usp.*
- [52] de Guevara M L L and Orellana P A 2006 *Phys. Rev. B* **73** 205303